2022 13th International Symposium on Communication Systems, Networks and Digital Signal Processing (CSNDSP) | 978-1-6654-1044-1/22/$31.00 ©2022 IEEE | DOI: 10.1109/CSNDSP54353.2022.9907907

Spectral Signature Multiplexing in Multispectral Camera Communication

Daniel Moreno
IDeTIC-ULPGC
Las Palmas de Gran Canaria, Spain
daniel.moreno@ulpgc.es

Victor Guerra
Pi Lighting
Sion, Switzerland
victor.guerra@pi-lighting.com

Julio Rufo
Universidad de La Laguna (ULL)
San Cristobal de La Laguna, Spain
jrufotor@ull.edu.es

Jose Rabadan
IDeTIC-ULPGC
Las Palmas de Gran Canaria, Spain
jrabadan@idetic.eu

Rafael Perez
IDeTIC-ULPGC
Las Palmas de Gran Canaria, Spain
rperez@idetic.eu

***Abstract*—Optical camera communication (OCC) is a technology foreseen to have a fundamental role in future communication applications due to the ubiquity of the cameras embedded in most consumer electronic devices and their increasing capabilities (high resolution, scanning frequency, *etcetera*). However, high-spectral-resolution cameras, such as multispectral cameras, present particular characteristics that can be exploited to provide new features to OCC links. Furthermore, as LED spectral responses are different when their temperature changes, more than one communication channel can be achieved using the same LED device if the camera can capture those modifications and distinguish the different LED spectral signatures due to the temperature variation. This novel approach is followed in this research, including some equalization techniques applied to the channel matrix to improve the extraction of the transmitted signal in the receiver reducing the inter-channel interference (ICI). This work shows that up to two distinct channels can be obtained with the same LED at different temperatures, getting a bit error rate (BER) below the forward error correction (FEC) limit.**

***Index Terms*—Optical camera communication, multispectral, light-emitting diodes, temperature effect.**

I. Introduction

OPTICAL camera communication (OCC) is attracting considerable interest due to the widespread use of cameras in smartphones, automobiles, surveillance, and healthcare, among others. The ubiquity of these devices and the recent advances in image sensors have boosted the uses of this technology in terms of research [1]. In addition, OCC has attracted the scientific community's attention in the last few years due to its potential immediate applications to the market. Recent developments have focused on employing novel modulation/demodulation techniques and different types of cameras and transmitters. Shiraki *et al.* developed a demodulation method using a Gaussian-mixture model to estimate the channel of the OCC system without any synchronization devices [2]. An LED-to-camera communication system based on color shift keying (CSK) was presented by Hu *et al.* [3]. They compared the throughput of several smartphone cameras and obtained a low symbol error rate avoiding color flicker.

Despite the vast amount of literature on OCC, the full potential of the technology has yet to be exploited, especially outside of conventional camera use. For example, some studies proposed using high-speed cameras to increase the data rate. Arai *et al.* put forward a hierarchical transmission scheme based on two-dimensional fast Haar wavelet transform to guarantee data detection when the camera is far from the transmitter [4]. Iwase *et al.* recognized a lighting pattern from a pattern-mixed image, setting the transmitting rate to the same receiver frame rate and reducing flickering by using 8B/10B encoding [5]. On the other hand, regarding the use of LEDs as transmitters, it is well-known that the spectral characteristics of LEDs are affected by temperature, which has a detrimental effect on the communication performance if not accounted for in the reception process [6], [7].

This work proposes an LED-to-camera communication using a multispectral camera as a receiver, which allows taking advantage of the numerous device bands to distinguish signals of different wavelengths. Furthermore, the LED spectral variation due to temperature is leveraged. Since the LED spectral response varies with thermal changes, those modifications can be grasped by a high-spectral-resolution camera. Therefore, new communication channels can be achieved utilizing the same transmitter device, as the LED spectral response modifies with temperature.

This paper is organized as follows. Section II gives a brief overview of OCC and presents the beneficial applications of using a multispectral camera as receiver in OCC. Section III examines the effect of temperature on LEDs. The procedures and techniques applied to carry out the experiments are described in Section IV. The results obtained from the methodology implemented are presented in Section V. Finally, some conclusions are drawn in Section VI.

This research was supported in part by the Universidad de Las Palmas de Gran Canaria's Trainee Predoctoral Research Staff Program (2019) and in part by the Spanish State Research Agency, project OCCAM PID2020-114561RB-I00.

II. Multispectral Camera Communication

OCC is a technology that employs an image sensor or a camera as an optical data receiver instead of a photodiode as used in visible light communication (VLC) links. Hence, one of the principal advantages of OCC is the ease with which cameras embedded in most consumer electronic devices can be used as receivers, permitting this type of OWC to be implemented without any requirement to add or modify the hardware. However, since these cameras are designed for photography, OCC's maximum achievable data rate is limited by the device's pixel clock and scanning method, allowing only low data rate transmissions [8].

Depending on the number of bands a camera can record and their width, the device's spectral accuracy would capture different signals from the same LED at different temperatures [9]. This effect is a fundamental aspect of this work and will be explained in-depth in Section III.

Regarding the channel modeling in OWC, the received power of an OCC system can be expressed as shown in Equation 1.

$$P_{rx} = P_{tx} R(\theta, \phi) \frac{A_{lens}}{d^2} \cos(\Psi), \tag{1}$$

where P_{tx} is the transmitted power, $R(\theta, \phi)$ is the source's radiation pattern at elevation θ and azimuth ϕ, A_{lens} is the main lens' cross section, d is the link range, and Ψ is the impact angle. As image-forming optics must be considered in OCC, neglecting any defocusing effect, the pixel power does not depend on distance when the projected size of the light source on the sensor is greater than one pixel (Equation 2).

$$A_{proj} = \frac{N_x N_y}{FOV_x FOV_y} \frac{A_{tx}}{d^2}, \tag{2}$$

A_{proj} is the projected number of pixels of the light source on the sensor, N_x and N_y define the sensor's pixel resolution, FOV_x and FOV_y are the camera's horizontal and vertical fields of view, respectively, and A_{tx} is the transmitter's effective area (from the receiver's viewpoint). These equations reveal that although P_{rx} decreases as distance increases, A_{proj} decreases as well (constant power density on the image sensor). Joining Equations 1 and 2, the received optical power at each pixel is obtained in Equation 3.

$$P_{px} = P_{tx} R(\theta, \phi) \frac{A_{lens}}{A_{tx}} \frac{FOV_x FOV_y}{N_x N_y} A_{px} \cos(\Psi), \tag{3}$$

where P_{px} is the pixel power (in watts) and A_{px} is the pixel area.

Regarding channel compensation, it is critical in any system subject to inter-channel interference (ICI). Several techniques aim to alleviate ICI, such as multiple-input multiple output (MIMO), wavelength division multiplexing (WDM) and CSK, which require an equalization stage to minimize the interference in VLC systems. Zero-forcing (ZF) and minimum mean square error (MMSE) equalizers are the usual algorithms applied to equalize [10]–[12].

ZF equalizer is a linear algorithm that reduces ICI to zero in a noiseless scenario. In multispectral camera communication (MCC), the channel matrix is formed by the responses of each camera band, i.e., the spectral signature. In most cases, this matrix could be non-square if the number of transmitters is different from the number of bands. For those cases, the Moore-Penrose pseudo-inverse (**W**) can be used to get the inverse channel matrix (Equation 4), which is applied to the received signal.

$$\mathbf{W}_{ZF} = \mathbf{H}^T \left(\mathbf{H} \cdot \mathbf{H}^T\right)^{-1}, \tag{4}$$

where **H** is the channel matrix and T indicates transposition.

On the other hand, MMSE equalizers are typically employed in communication systems instead of ZF ones since they take into consideration the noise in the system to optimize the output signal-to-noise ratio (SNR). Equation 5 reveals the calculation of the matrix that is used to make the received signal close to the transmitted signal.

$$\mathbf{W}_{MMSE} = \mathbf{H}^T \left(\mathbf{H} \cdot \mathbf{H}^T + \frac{1}{SNR} \cdot \mathbf{I}\right)^{-1}, \tag{5}$$

where **I** is the identity matrix. It can be noted from Equation 5 that for high SNR values, the Moore-Penrose inverse used in ZF equalization (Equation 4) and the matrix used in MMSE are equivalent.

On the other hand, the received signal y can be represented as:

$$y = \mathbf{H} \cdot x + n, \tag{6}$$

where x is the transmitted signal and n is additive white Gaussian noise (AWGN). Once the compensation matrix **W** is calculated, introducing the linear compensation in Equation 6 yields an estimation of the transmitted signal (Equation 7).

$$\hat{x} = \mathbf{W} \cdot (\mathbf{H} \cdot x + n) \tag{7}$$

It must be considered that regardless of the estimation mechanism of **W**, its components will be subject to AWGN. Therefore, the compensation mechanism will not be ideal, and an estimation of the compensation performance is needed. In this regard, the condition number of the channel matrix can be used as this performance metric, as shown in [9] (Equation 8). Well-conditioned matrices (values close to one) better estimate the transmitted signal than ill-conditioned ones (values much higher than one).

$$\text{cond}(\mathbf{H}) = \|\mathbf{H}\| \cdot \|\mathbf{H}^{-1}\| \tag{8}$$

III. Thermal effects on LED devices

The impact of temperature on LED devices has been extensively investigated in the literature. It is well-documented that the efficiency and the spectral characteristics of these light sources are severely affected by variations in the p-n junction temperature.

The energy gap of the semiconductor materials depends on the junction temperature, as modeled in Equation 9 [13]. Generally, the energy gap decreases as temperature increases. Thus, since the energy is inversely proportional to the wavelength (Planck-Einstein relation), the latter increases with temperature causing a variation in the LED emission.

$$E_g = E_0 - \frac{\alpha T^2}{T + \beta}, \tag{9}$$

where T is temperature, E_0 is energy gap at $0\,\mathrm{K}$ temperature condition, and α and β are semiconductor-dependent constants, which are empirically determined.

As regards photometric parameters, in [14], surface mount device (SMD) LED's optical parameters were measured at various temperature conditions. It revealed that the peak wavelengths were expectedly red-shifted as temperature increased. Besides, intensity, spectral width, and color-coordinates shift were affected. In addition, luminous flux and efficacy on LEDs were analyzed at different operating conditions in [15]. Based on the fact that luminous flux and efficacy decrease as junction temperature grows, the authors determined the optimized conditions of the LEDs.

Considering the temperature effects mentioned above, this work proposes taking advantage of the thermal impact on LEDs, especially those concerning spectral changes, to utilize a multispectral camera that captures the variation. Thus, by inducing a controlled temperature to the LED would be possible to have the same light source with a different spectral signature. As a result, this spectral variation could be used to implement several communication channels in an OCC link with a multispectral camera as a receiver.

IV. Methodology

The basic concept of the experiment was to use pairs of the same LED model and change their p-n junction temperature by the Joule effect to obtain different spectral responses. Thus, each LED had a specific spectral signature that a multispectral (MS) camera could capture. Furthermore, in order to have those different signatures, each LED had distinct pulse-width modulation (PWM) duty cycle (DC) values so that the higher the DC value, the higher the junction temperature. No thermal management techniques, such as heat sinks, were used in this work, as they would reduce the variation of the LED spectral characteristics. Once the desired temperature was reached, the data transmission started, the camera captured the images, and, finally, the system's performance was evaluated. Taking the aforementioned explanation into account, Fig. 1 depicts the three main phases of the experiment.

In the first phase, several LED p-n junction temperatures must be achieved. Therefore, the LEDs were set with 30% and 70% of DC values. The frequency of the PWM was set to 5 Hz (bit time of 200 ms). In order to reach the thermal steady state on the LEDs, before sending data, the transmitters were set to an idle state for 5 minutes because no external thermal management technique was applied to

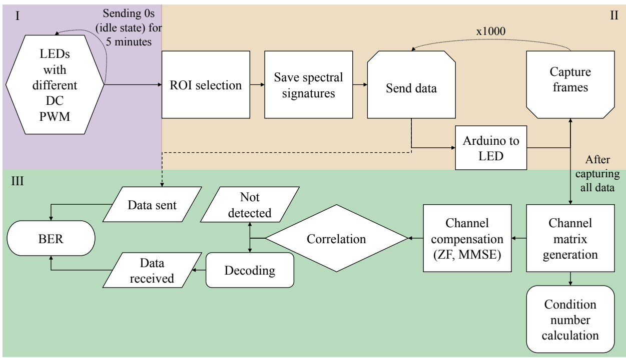

Fig. 1. Flow diagram of the methods. It is divided into three phases. Phase I: stabilization of the LED temperature. Phase II: transmission and reception. Phase III: performance evaluation.

stabilize the temperature. It consisted of keeping the LEDs sending a binary zero with the corresponding DC.

During the second phase, the region of interest (ROI), where the light beams of the LEDs were mixed, was selected. Then, the channel matrix was estimated by capturing the spectral responses of each LED. After that, the transmission began. On the other hand, data transmission was based on the following steps. Firstly, a list of 1000 8-bit pseudo-random integers was generated for each transmitter. Next, the elements of each list were sent to the micro-controller devices in byte format. However, the generated bit sequence was 8B/10B encoded in the micro-controller part. Due to the sensitivity of the spectral signature to temperature, it was essential to avoid long sequences of "1" or "0". Therefore, the applied encoding allowed a header comprising non-consecutive "0" and "1". Moreover, the same header was added after the payload to improve the frame-detection process.

Regarding the MS camera, it has eight narrow bands whose center wavelengths are, from band 1 to band 8: 424, 464, 504, 544, 573, 614, 656, and 699 nm, respectively. Besides, it possesses one panchromatic band that covers the wavelength range from 400 to 800 nm (band 9). The MS camera's frame rate was set to 50 frames per second (fps) and working mode to global shutter. These parameters would allow capturing every 20 ms, so, as the bit time was 200 ms, it permitted ten samples per bit. Although the orchestration script synchronized transmission and data capture, a guard period was added before and after data transmission to ensure that the whole bit stream (header + payload + footer) was captured. Those frames were stored in a ring buffer and saved individually per every data sent. As for the exposure, the aperture setting was f/2.4, the maximum allowed by the lens, and the exposure time varied according to the LEDs used (Table I) with the purpose of not saturating the camera with the signals.

Finally, once all the data were taken, the third phase evaluated the system performance. It began with the generation of the channel matrix. The spectral signatures of each LED were normalized by their maximum values and added to the matrix so that it had one signature per row. Alternatively, the condition number of the matrix was

TABLE I
EXPERIMENT KEY PARAMETERS.

Parameter	Value
	Transmitter
Light sources	Kingbright L-53SRC-C (Red) Kingbright L-154A4SUREQBFZGEW (Green, Blue)
Dominant wavelengths [nm]	660 (Red), 520 (Green), 460 (Blue)
Control device	Arduino UNO
	Receiver
Camera	SILIOS Technologies CMS-C1-C-EVR1M-GigE
Resolution [px]	1280×1024 (raw image) 426×339 (multispectral images)
Exposure time [ms]	20 (Red), 6.5 (Green), 0.25 (Blue)
Aperture	f/2.4
Frame rate [fps]	50
Shutter mode	Global shutter
	Bit stream
Coding	8B/10B
Modulation	VPPM
Bit time [ms]	200
Duty cycle	30%, 70%
Bits	Header: 10, Payload: 8, Footer: 10

TABLE II
CONDITION NUMBER OF THE CHANNEL MATRICES.

	R	G	B
Condition number (dB)	24.10	31.29	31.18

calculated as a metric of its performance. Following this, the channel matrix was compensated by applying ZF and MMSE algorithms. At this point, the mixed signals were consequently split into two signals. The resulting signals were then correlated with a matrix comprising all available transmitted signals.

Given that the length of the transmitted signal (header + payload + footer) was shorter than the length of the received signal because the latter included extra frames to avoid missing information, the correlation was performed traversing the template signals through the received signal. As soon as the correlation had been done, the maximum value was then taken. Before decoding the signal, in order to prevent getting a large number of bit errors, a correlation threshold was established. The bit stream was deemed undetected if the maximum coefficient was less than the threshold. Otherwise, if it was greater than the threshold, the received signal was decoded and compared to the sent signal obtaining the bit error rate (BER). The procedure was replicated for several thresholds ranging from 0 to 0.95. Lastly, the whole process was repeated for each LED pair. Table I summarizes the experiment key parameters.

V. RESULTS

Table II compares the condition numbers of all the matrices employed in this work. It is divided into three columns corresponding to the RGB LEDs. It can be seen that the red LED obtained the lowest values, indicating that the spectral response curves of this color are the most separable ones. For the green and the blue LEDs, both obtained similar results. It is mathematically proved because condition number tends to infinity if a spectral signature is close to a linear combination of others. Therefore, the matrices comprising the spectral responses of LEDs at different temperatures whose variability from each other is not significant would be worse conditioned than those

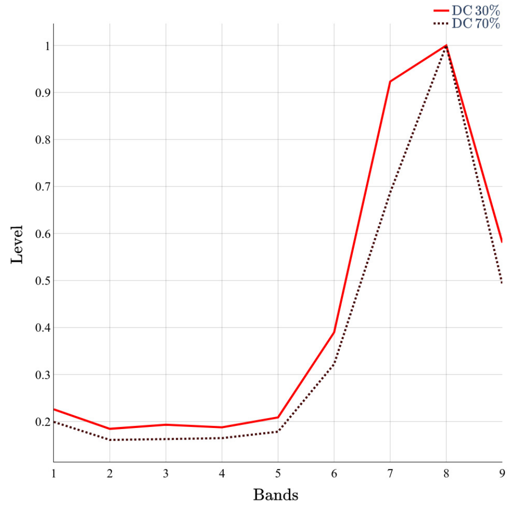

Fig. 2. Normalized spectral signatures of the red LEDs at different temperatures. Solid and dotted lines correspond to the LEDs working at 30% and 70% DC values, respectively.

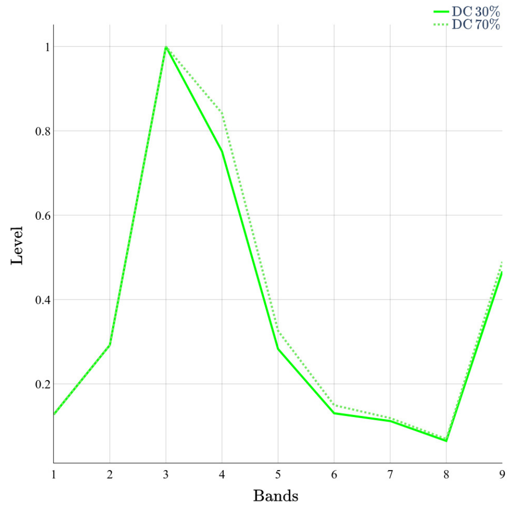

Fig. 3. Normalized spectral signatures of the green LEDs at different temperatures. Solid, and dotted lines correspond to the LEDs working at 30% and 70% DC values, respectively.

matrices formed by the spectral signatures of LEDs with considerable variability.

Figs. 2, 3, and 4 show the spectral signatures of the three LEDs (red, green, and blue, respectively) at different temperatures (several DC values). The x-axis represents the spectral bands, whereas the y-axis represents the normalized camera level. It can be seen that the responses of the red LEDs showed the highest variability from each other, while the green and the blue LEDs presented a higher similarity, respectively.

The system performance for two transmitters is presented in Fig. 5. These pinpoint the BER and the not detected bit streams based on the imposed correlation threshold. The algorithm employed for the channel compensation to obtain these results was the ZF. The MMSE

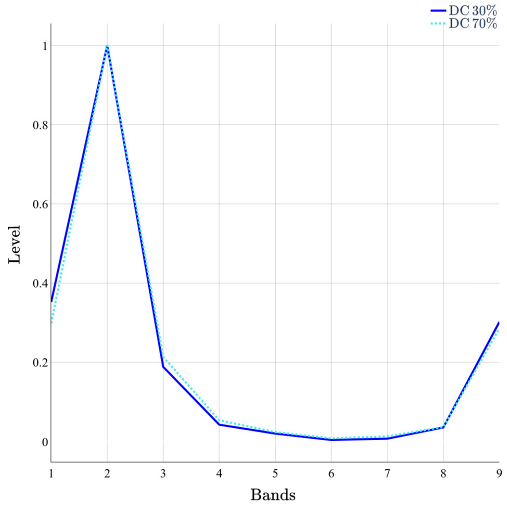

Fig. 4. Normalized spectral signatures of the blue LEDs at different temperatures. Solid and dotted lines correspond to the LEDs working at 30% and 70% DC values, respectively.

results were omitted in this paper because they showed similar performance to the ZF due to the high SNR of the link.

As far as the performance analysis is concerned, the best outcome was obtained for the red LEDs, followed by the green and blue LEDs, as expected. It can be noted from Fig. 5a that the BER of the red LEDs was approximately 10^{-2} for the LEDs at 30% and 70% from thresholds of 0 to 0.25. Besides, from the correlation thresholds of 0.5 and 0.6, the BER was below the forward error correction (FEC) limit ($3.8 \cdot 10^{-3}$) for the LEDs at 30% and 70%, respectively. Using those thresholds, the LEDs reached a BER just under $3.5 \cdot 10^{-3}$, and about 3% of the bit streams were not detected. From the thresholds of 0.85 and 0.9, none of the bit streams were detected for the LEDs at 30% and 70%, respectively.

For the green LEDs (Fig. 5b), the one at 30% got a BER of about $4.7 \cdot 10^{-2}$ for the lower threshold values. It reached a BER below the FEC limit from the thresholds greater than 0.75, reaching a BER of $2.5 \cdot 10^{-3}$ with 17% of the bit streams not detected. The LED at 70% achieved better BER performance than its peer with $3.2 \cdot 10^{-2}$ for the lower threshold values. The BER below the FEC limit was reached from thresholds greater than 0.7. Its most striking results were a BER of $3.7 \cdot 10^{-3}$ and approximately 10% of the bit streams not detected. At a threshold of 0.95, the LED at 30% did not detect the majority of the bit streams, while the LED at 70% missed approximately 35% of them. In the case of the blue LEDs (Fig. 5c), their performance was unsuccessful in getting BER below the FEC limit. On the one hand, the LED at 30% got a BER of $3.3 \cdot 10^{-3}$, missing just over 40% of the bit streams at a threshold of 0.85. On the other hand, the LED at 70% got a BER of about 10^{-4}, discarding more than 90% of the bit streams at a threshold of 0.55. Table III highlights the results above mentioned.

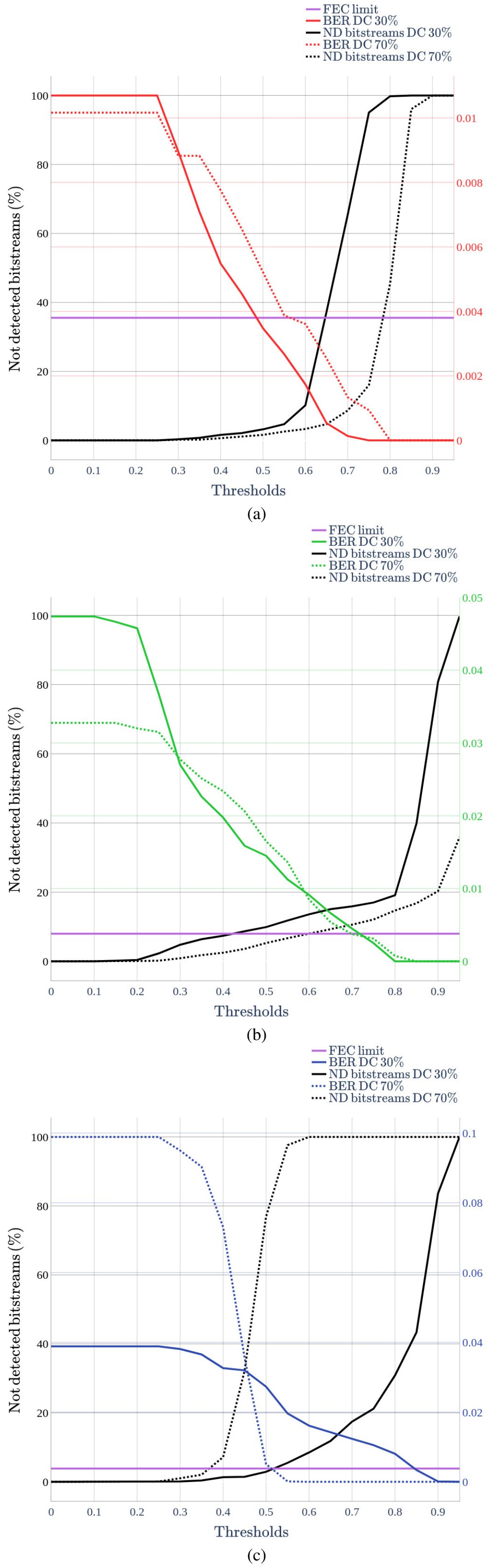

Fig. 5. BER and not detected bit streams at different detection thresholds corresponding to the pairs of (a) red, (b) green, and (c) blue LEDs. Solid and dotted lines correspond to the LEDs working at 30% and 70% DC values, respectively.

TABLE III
LED'S PERFORMANCE COMPARISON

LEDs	DC	BER below FEC limit	Undetected bit streams	Threshold
Red	30%	$3.48 \cdot 10^{-3}$	3.21%	0.50
	70%	$3.61 \cdot 10^{-3}$	3.32%	0.60
Green	30%	$2.50 \cdot 10^{-3}$	17.00%	0.75
	70%	$3.75 \cdot 10^{-3}$	10.60%	0.70
Blue	30%	$3.38 \cdot 10^{-3}$	43.35%	0.85
	70%	$1.30 \cdot 10^{-4}$	97.61%	0.55

VI. Conclusions

In this research, an experimental OCC link was carried out utilizing a multispectral camera as a receiver. Furthermore, the spectral features of the LEDs employed as transmitters were altered by modifying their p-n junction temperature. Thus, the same LED model would provide different spectral behaviors, which the MS camera would exploit. The LED temperatures were varied because of the Joule effect by supplying various driving currents to the LEDs. No heat sink was used in this work since it would have reduced the thermally-induced spectral variation of the LEDs. Pairs of LEDs with different dominant wavelengths have been used, and their performance has been analyzed.

The strength of this study lies in reaching new channels from the same emitter by changing its temperature. A high-spectral-resolution camera such as a multispectral camera allows grasping the subtle differences in the LED spectral responses. The obtained results prove that BER below the FEC limit can be achieved for those LEDs whose spectral features are considerably affected by thermal changes. It is also fundamental to note that a retransmission approach must be followed for those cases where the bit streams were not detected.

On the other hand, the performance was somewhat disappointing for the green and the blue LEDs. The prime cause of these undesired results is a consequence of the temperature impact on those light sources. In contrast to the red device, whose peak wavelength was considerably red-shifted, the green and the blue LEDs were less affected by thermal changes. Those results were evidenced in the condition number of their matrices, achieving the worst outcomes for those with greater values. Therefore, the findings of this research suggest that using optical emitters whose spectral characteristics are more affected by thermal variations would improve the achievement of the experiment. However, a trade-off between the degree of spectral variation and the decrease in efficiency caused by temperature must be considered in a scenario where the light sources would be used for both illumination and communication purposes.

The present findings imply that multispectral cameras could be taken advantage of in order to exceed the number of channels that an LED can reach by exploiting the temperature effects on its spectrum.

On a broader level, a combination of LEDs with different dominant wavelengths can be used. Thus, the camera bands centered on a particular wavelength would help to separate the signals following the procedure applied in this study. Moreover, the prospect of using the thermal effects on LEDs serves as a continuous stimulus for future research. For instance, characterization of various emitting devices could be performed, both the same model as different ones, to analyze the usefulness of each device in this approach.

References

[1] M. Z. Chowdhury, M. Shahjalal, M. K. Hasan, and Y. M. Jang, "The role of optical wireless communication technologies in 5g/6g and iot solutions: Prospects, directions, and challenges," *Applied Sciences*, vol. 9, no. 20, 2019. [Online]. Available: https://www.mdpi.com/2076-3417/9/20/4367

[2] Y. Shiraki, T. G. Sato, Y. Kamamoto, T. Izumi, Y. Nakahara, K. Kondo, and T. Moriya, "A demodulation method using a gaussian mixture model for unsynchronous optical camera communication with on-off keying," *Journal of Lightwave Technology*, vol. 39, no. 6, pp. 1742–1755, 2021.

[3] P. Hu, P. H. Pathak, H. Zhang, Z. Yang, and P. Mohapatra, "High speed led-to-camera communication using color shift keying with flicker mitigation," *IEEE Transactions on Mobile Computing*, vol. 19, no. 7, pp. 1603–1617, 2020.

[4] S. Arai, S. Mase, T. Yamazato, T. Endo, T. Fujii, M. Tanimoto, K. Kidono, Y. Kimura, and Y. Ninomiya, "Experimental on hierarchical transmission scheme for visible light communication using led traffic light and high-speed camera," in *2007 IEEE 66th Vehicular Technology Conference*, 2007, pp. 2174–2178.

[5] D. Iwase, M. Kasai, T. Yendo, S. Arai, T. Yamazato, H. Okada, and T. Fujii, "Improving communication rate of visible light communication system using high-speed camera," in *2014 IEEE Asia Pacific Conference on Circuits and Systems (APCCAS)*, 2014, pp. 336–339.

[6] E. Tugcu, A. Yazgan, C. Albayrak, and K. Turk, "Red-shift effect in multi-color leds based visible light communication," *Optics Communications*, vol. 463, p. 125451, 2020. [Online]. Available: https://www.sciencedirect.com/science/article/pii/S0030401820301115

[7] D. Moreno, J. Rufo, V. Guerra, J. Rabadan, and R. Perez-Jimenez, "Effect of temperature on channel compensation in optical camera communication," *Electronics*, vol. 10, no. 3, 2021. [Online]. Available: https://www.mdpi.com/2079-9292/10/3/262

[8] W. A. Cahyadi, Y. H. Chung, Z. Ghassemlooy, and N. B. Hassan, "Optical camera communications: Principles, modulations, potential and challenges," *Electronics*, vol. 9, no. 9, 2020. [Online]. Available: https://www.mdpi.com/2079-9292/9/9/1339

[9] D. Moreno, J. Rufo, V. Guerra, J. Rabadan, and R. Perez-Jimenez, "Optical multispectral camera communications using led spectral emission variations," *IEEE Photonics Technology Letters*, vol. 33, no. 12, pp. 591–594, 2021.

[10] Y. S. Hussein, M. Y. Alias, and A. A. Abdulkafi, "On performance analysis of ls and mmse for channel estimation in vlc systems," in *2016 IEEE 12th International Colloquium on Signal Processing Its Applications (CSPA)*, 2016, pp. 204–209.

[11] A. Anusree and R. K. Jeyachitra, "Performance analysis of a mimo vlc (visible light communication) using different equalizers," in *2016 International Conference on Wireless Communications, Signal Processing and Networking (WiSPNET)*, 2016, pp. 43–46.

[12] M. K. Jha, N. Kumar, and Y. V. S. Lakshmi, "Noma mimo visible light communication with zf-sic and mmse-sic," in *2020 2nd PhD Colloquium on Ethically Driven Innovation and Technology for Society (PhD EDITS)*, 2020, pp. 1–2.

[13] Y. P. Varshni, "Temperature dependence of the energy gap in semiconductors," *physica*, vol. 34, no. 1, pp. 149–154, 1967.

[14] M. E. Raypah, M. Devarajan, and F. Sulaiman, "Influence of injection current and ambient temperature on intensity and wavelength of low-power smd led," in *2016 IEEE 37th International Electronics Manufacturing Technology (IEMT) 18th Electronics Materials and Packaging (EMAP) Conference*, 2016, pp. 1–6.

[15] M. E. Raypah, B. K. Sodipo, M. Devarajan, and F. Sulaiman, "Estimation of luminous flux and luminous efficacy of low-power smd led as a function of injection current and ambient temperature," *IEEE Transactions on Electron Devices*, vol. 63, no. 7, pp. 2790–2795, 2016.